Strong-bonding hole-transport layers reduce ultraviolet degradation of perovskite solar cells

Chengbin Fei[1], Anastasia Kuvayskaya[2], Xiaoqiang Shi[1], Mengru Wang[1], Zhifang Shi[1], Haoyang Jiao[1], Timothy J. Silverman[3], Michael Owen-Bellini[3], Yifan Dong[4], Yeming Xian[5], Rebecca Scheidt[4], Xiaoming Wang[5], Guang Yang[1], Hangyu Gu[1], Nengxu Li[1], Connor J. Dolan[6], Zhewen JD Deng[6], Deniz N. Cakan[6], David P. Fenning[6], Yanfa Yan[5], Matthew C. Beard[4], Laura T. Schelhas[3], Alan Sellinger[2,4] and Jinsong Huang*[1,7]

[1]Department of Applied Physical Sciences, University of North Carolina at Chapel Hill, Chapel Hill, NC 27599, USA

[2]Department of Chemistry, Colorado School of Mines, Golden, CO, USA

[3]Materials Chemicals and Computational Science Directorate, National Renewable Energy Laboratory, Golden, CO 80401 USA

[4]Chemistry and Nanoscience Center, National Renewable Energy Laboratory, Golden, CO 80401, USA

[5]Department of Physics and Astronomy, University of Toledo, Toledo, OH 43606, USA

[6]Department of Nanoengineering, University of California, San Diego, La Jolla, CA 92093, USA

[7]Department of Chemistry, University of North Carolina at Chapel Hill, Chapel Hill, NC 27599, USA

Corresponding author: jhuang@unc.edu (J. H.)

Abstract

The light-emitting diodes (LEDs) used in indoor testing of perovskite solar cells do not expose them to the levels of ultraviolet (UV) radiation they would receive in actual outdoor use. We report degradation mechanisms of p-i-n structured perovskite solar cells under unfiltered sunlight and with LEDs. Weak chemical bonding between perovskites and polymer hole transport materials (HTMs) and transparent conducting oxides (TCOs) dominate the accelerated A-site cation migration, rather than direct degradation of HTMs. An aromatic phosphonic acid, [2-(9-ethyl-9H-carbazol-3-yl)ethyl]phosphonic acid (EtCz3EPA) enhanced the bonding at the perovskite/HTM/TCO region with phosphonic acid group bonded to TCOs and nitrogen group interacting with lead in perovskites. A hybrid HTM of EtCz3EPA with strong hole extraction polymers retained high efficiency and improved the UV stability of perovskite devices, and a champion perovskite minimodule, independently measured by Perovskite PV Accelerator for Commercializing Technologies (PACT) center, retained operational efficiency >16% after 29 weeks of outdoor testing.

Introduction

Perovskite solar cells (PSCs) with high power conversion efficiency (PCE) and improved durability and scalability have been reported (*1-3*). Some devices have reach T_{90}, the time to a 10% drop in (PCE), of > 10,000 hours of light exposure, not only for small perovskite cells, but also for perovskite minimodules (*4*). Several strategies were also reported to retain > 90% of their initial PCE after the light exposure tests at high temperature of 85 ºC for > 1000 hr (*5-7*). However, almost all of the light-soaking stability tests were conducted using inorganic light-emitting diodes (LEDs) as light sources that do not have a substantial ultraviolet (UV) component (*2, 8-11*). There is no demonstration of outdoor stability showing perovskite modules with area > 15 cm^2 that still have an aperture efficiency > 15% after 10 weeks of outdoor testing. Thus, a huge gap exists between the indoor and outdoor durability testing results, and much improved outdoor durability is needed. Although it is possible to completely or partially block UV light using UV-filter layers or down-conversion luminescent materials (*12*), they may suffer from instability issues including wear over years, or the increased cost and sacrificed energy yield.

Outdoor conditions are different from indoor light-soaking or maximum power point (MPP) tracking in several ways. Temperature, irradiance, and UV light intensity constantly change outdoors. We speculate that the indoor-outdoor durability gap mainly comes from the lack of or weak UV light from most LED lamps for indoor tests, because perovskite devices are frequently reported to pass the IEC61215 thermal cycling test (*13-15*). UV light has been reported to accelerate the degradation of perovskite solar cells, but there is still no consensus yet on the mechanisms. Photocatalytic effects have been considered as the main reason for UV-induced perovskite degradation in n-i-p structured perovskite solar cells with TiO_2 (*16*) and SnO_2 (*17*) as electron-transport layers. The UV light generated electrons in TiO_2 were reported to convert adsorbed oxygen on TiO_2 into hydroxyl radicals which oxidize I^- to I_2 (*18*). Another study suggested UV light could directly activate oxygen vacancies and the cations in TiO_2 and SnO_2, prompting the accumulation of I_3^- (*19*). In p-i-n structured devices, UV light was also reported to directly breakdown the chemical bonds in the organic hole-transporting materials (HTM), such as poly[bis(4-phenyl)(2,4,6-trimethylphenyl)amine] (PTAA), and thus introduced charge-trapping defects (*20, 21*).

Here, we investigate the mechanism of UV light-induced degradation in p-i-n structured PSCs with organic HTMs and develop a method to narrow down the gap between indoor and outdoor durability. The trap density of the perovskite/indium tin oxide (ITO) superstrate interface in the devices increased with exposure under UV light and generated more positively charged iodine interstitials, which accelerated the cation migration and phase segregation at the buried perovskites/ITO interface. Using the new HTM with improved bonding in the PSCs, the perovskite/ITO interface was stabilized that were then used in minimodules with demonstrated record outdoor stability.

Solar cell degradation mechanism under outdoor test

To evaluate the indoor and outdoor durability, we fabricated small-area devices with a p-i-n structure of ITO/PTAA/$FA_{0.9}Cs_{0.1}PbI_3$/C_{60}/bathocuproine(BCP)/Cu, where ITO is indium tin oxide, PTAA is poly[bis(4-phenyl)(2,4,6-trimethylphenyl)amine, and FA is formamidinium (**Fig. S1A**). The spectra of lamps used for light-soaking stability evaluation is shown in **Fig. S2** together with the solar spectrum. The UV light in most commercial LED lamps for the indoor testing was found to be extremely weak, constituting < 0.1% of total light, far lower than the 4.6% UV light in the solar spectrum. After light soaking under a LED lamp at 60±5 ºC and open-circuit (OC) conditions for ~200 hr, these optimized devices with a polyisobutylene (PIB) blanket encapsulation retained ~103% of the initial (PCE) (**Fig. 1A**), consistent with our prior results (*2, 22*). However, outdoor devices with the same encapsulation were tested under open-circuit (OC) conditions in North Carolina, US in October 2021, when there was an averaged temperature of ~20 ºC in daytime (**Fig. S1**), showed a rapid reduction in PCE by ~21% after 10 days. The degradation of devices was mainly from the reduced short-circuit current density (J_{SC}) and fill factor (FF).

The main difference between the indoor and outdoor tests should be the temperature, light source, and the light cycling. Temperature is likely not the key factor difference because the outdoor temperature was even lower than indoor temperature. In addition, our recent study showed that the small area devices using the same device structure could last > 3000 hr under light exposure tests at 60±5 ºC (*2*). After 35 cycles of standard light cycling (ISOS-LC-1) testing (*23*) (**Fig. S3**), the devices kept ~105% of initial PCE, which excludes the light cycling as the main reason for the fast outdoor degradation. Thus, the higher UV component in sunlight is likely the main reason for faster degradation. We used a light emission plasma (LEP) lamp to simulate sunlight which contains 3.5% UV light (**Fig. S2C**). After covering the devices with a long-pass optical filter with a cut-off wavelength of 435 nm, the rapid degradation disappeared at the initial stage (**Fig. S4**), confirming that UV light is likely responsible for the accelerated device degradation in the outdoor test.

UV light may damage primary chemical bonds in PTAA, perovskites, or the secondary bonding at the ITO/PTAA/perovskite region. To pinpoint which dominates the UV-induced device degradation, PTAA powder was exposed to a UV lamp (390 to 400 nm) with a light intensity of 10 mW cm^{-2} in N_2 atmosphere for ~200 hr, and the UV-irradiated PTAA powder was used for device fabrication (**Fig. S5A**). Absorption spectra change of PTAA was used to characterize the degree of damage to the PTAA layer by UV light illumination (**Fig. S5B**). PTAA shows an absorption in the wavelength range < 425 nm. The absorption peak of the PTAA film prepared from UV-irradiated PTAA was reduced by ~45% and showed obvious UV damage. However, devices prepared using the UV-irradiated PTAA only lost 0.5% of their PCE compared to the reference devices (**Fig. S5C**), which was 1/10 of the reduction in **Fig. 1A** and is mainly from the open-circuit voltage (V_{OC}) reduction. The PCE loss in the outdoor test was dominated by the reduction of J_{SC} and FF, suggesting a different degradation mechanism.

We then checked the perovskite film stability and PCE evolution with In^{3+} surface processing, because In^{3+} ions in ITO have been hypothesized to leach into the perovskite under

UV treatment and cause perovskite damage (*24, 25*). As shown in **Fig. S6**, the perovskite films with $InBr_3$ surface treatment did not show faster color changes (yellowing) under LEP lamp than samples with FABr surface treatment. The device durability showed a similar trend, indicating In^{3+} unlikely introduced additional perovskite damage. Therefore, the accelerated degradation in outdoor test comes from either fast degradation of perovskite itself or the breakdown of the weak interface between perovskites and the underlying ITO/PTAA substrates.

The ITO side of the PSCs changed from a dark color initially to gray after the ~200 hr test under LEP light (3.5% UV, ~100 mW cm^{-2}, 60±5 ºC, OC conditions), indicating changes in the perovskite layer (**Fig. 1B**). To understand the material change, we performed transient reflectance spectroscopy (TR) analysis on perovskite films before and after light soaking. The perovskite films were deposited on ITO/PTAA substrates and illuminated from ITO side. The perovskite film was excited and probed from the top side (perovskite/air) and bottom side (ITO/PTAA) with a pump laser wavelength of 400 nm, which penetrates < 50 nm into perovskites (**Fig. 1, C to E**). In TR experiments, the light only probes ~20 nm of the perovskite and with short wavelength excitation. The fast initial decay of the amplitude represents carriers moving out of the probing region (carrier diffusion from the surface to the bulk), and the longer time kinetics represents the total carrier density decay reflecting both surface and bulk recombination. We observed no change of the fast decay when light entered from the perovskite/air side, which indicates no degradation of perovskite within the probing region at the top surface.

The longer time decay improved after 300 hr of LEP exposure, which most likely the result of improved surface recombination. During probing the perovskite/PTAA/ITO side, notable slower decay in the fast component underwent noticeably slow decay after 300 hr, indicating that a large reduction in carrier mobility (slower carrier diffusion away from the surface) occurred in perovskite film near the PTAA side after photodegradation. As shown in **Fig. S7** and **Table S1**, the grazing incident x-ray diffraction (GIXRD) was also conducted from the top surface of the photodegraded perovskite films with different incident angles (ω). With the increase of ω from 0.3º to 1º that resulted in increased x-ray penetration depth, the ratio of yellow phase and black phase perovskite increased by ~90%, confirming the faster degradation of perovskites near the PTAA side.

We studied both top and bottom interfaces with incident blue excitation light from both sides of the perovskite films before and after 100 hr of illumination under LEP lamp. At the perovskite film bottom, many dark spots appeared after illumination in the photoluminescence (PL) intensity mapping images (**Fig. 1F**). The optical bandgap mapping by tracking PL emission peak showed that the illuminated films became more nonuniform (**Fig. 1G**), which confirmed phase segregation induced by cation migration in $FACsPbI_3$. For the perovskite top surface, the changes in PL intensity and bandgap mapping were much smaller after illumination (**Fig. S8A**, **S8B**). Thus, degradation under LEP lamp started from PTAA side and was induced by cation migration. The PL peak position of the fresh samples at the top side blue-shifted by 3 nm compared to the bottom side (**Fig. S8D**), which reflected different Cs ratio in the vertical direction in this composition (*26*).

Scanning electron microscope (SEM) images revealed that several needle-shaped regions emerged at the bottom of the perovskite films (**Fig. 1G**), which was different from the morphology of pristine $FA_{1-x}Cs_xPbI_3$. Similar morphologies were also observed in x-ray fluorescence (XRF) mapping (**Fig. 1H**), where these needle regions had higher Cs/I element ratios and pronounced segregation of A-site cations. A weak phase segregation was also observed in $FA_{1-x}Cs_xPbI_3$ under the LED lamp by PL mapping but only after 2000 to 3000 hr (**Fig. S8C**). The more severe and faster phase segregation under the LEP lamp indicates that UV light accelerated the migration of A-site cations and phase segregation by > 10 times.

To understand why and how UV light accelerated the phase separation of A-site ions, we studied the evolution of J-V curves (where V is voltage) and the trap density in the devices with PTAA as HTM. The samples were exposed to LEP light with a light intensity of 100 mW cm^{-2} at ~60 ºC. With increased light exposure time from 0 to 20 hr, the PCE of the devices decreased monotonically (**Fig. 2A**). The trap density of state (tDOS) of the devices was measured by thermal admittance spectroscopy (TAS), and typically exhibited three distinct trap bands (I, II and III), representing I_i^-, I_i^+ defects, and defect related to amorphous regions near the bottom interface, respectively, in iodide-based perovskite solar cells (*27, 28*). As shown in **Fig. 2B**, defects in all trap bands monotonically increased, which is consistent with the trend in the PCE reduction of the device. The initial large background I_i^- density made the change less distinct for I_i^+ defects. Nevertheless, the dramatic increase of already high-density trap band III indicated the perovskites near the bottom interface became much more amorphous. **Fig. 2C** shows the variation of tDOS of the devices made in the same batch but exposed to LED lamps of the same light intensity. Only a very small change in trap band II was observed, but no notable change was observed for trap band I and III.

The temperature-dependent dark conductivity was also measured to evaluate ion migration near the bottom perovskites. To measure the ion migration near the bottom interface, a narrow (30 μm) channel was formed by etching ITO so that we could evaluate the lateral ion migration with the device structure shown in **Fig. 2D**. After 50 hr illumination under LEP lamp, the derived ion migration activation energy (E_a) decreased from 410 to 266 meV, indicating the accelerated ion migration near ITO/PTAA/perovskite interface region after aging. All of these studies showed that the UV light-induced degradation of device was caused by damage in this region.

We hypothesize that the weak interaction of perovskites with PTAA and ITO at the bottom is adversely affected by UV light and makes the buried perovskite interface resemble the top perovskite surface. The formation of dangling bonds (*29*) resulted in faster ion migration at the bottom of the perovskite films and accelerated the phase segregation, breaking down the crystal and generating more point defects. The I_i^+ defects could trap photogenerated electrons and leave excess holes for the devices under illumination. Excess holes have been shown to accelerate the migration of the A-site cations (*30*), and eventually lead to segregation of cations at the bottom of perovskite films (**Fig. 2E**).

Enhancing UV and outdoor stability using bilateral bonding HTMs

Based on this hypothesis, enhancing the interaction of perovskites with ITO and HTM is needed to improve devices' UV and thus outdoor stability. We chose linker molecules that could anchor to ITO at one end and bond to perovskites at the other end (**Fig. 3A**). As shown in **Fig. S9**, several new and existing molecules were selected as linkers and used to replace the PTAA or form linker/PTAA hybrid layer structure as HTM, including a new molecule [2-(9-ethyl-9H-carbazol-3-yl)ethyl]phosphonic acid (EtCz3EPA) and well-studied [2-(9H-carbazol-9-yl)ethyl]phosphonic acid (2PACz) (*10, 31-34*). The acid groups such as -COOH and -$PO(OH)_2$ can be linked to the OH groups on ITO substrate, whereas -NH-, =O, halide (-X) and carbazole group can interact with Pb^{2+} in the perovskites.

The chemical structure, synthesis route, and characterizations of EtCz3EPA are shown in **Fig. 3B** and **Fig. S10**. The EtCz3EPA synthesis used inexpensive chemicals, mild reaction conditions, and simple purification steps. EtCz3EPA had similar carbazole and phosphonic acid groups as 2PACz, but the side chain with the phosphonic acid group was directly linked to the aromatic rings rather than N in the carbazole. Density functional theory (DFT) calculations (**Fig. S11**) showed that the carbazole group in 2PACz prefers to align normal to the perovskite surface, and had a small binding energy of 0.259 eV with perovskites. In contrast, the carbazole group in EtCz3EPA with an ethyl group preferred to stay in-plane direction, which allowed for better interaction of N with Pb^{2+} in perovskite. The binding energies of EtCz3EPA on the (111) plane of In_2O_3 surface and the (001) plane of $FAPbI_3$ surface are 0.70 eV and 0.78 eV stronger, respectively, than that of 2PACz. The use of the EtCz3EPA molecule as an interfacial binder is expected to reduce the formation of point defects at the buried interface and suppress UV-induced degradation. The device fabricated with EtCz3EPA also exhibited higher PCEs and improved stability under the LEP lamp compared to the other molecules tested in this study (**Fig. S12**), we selected EtCz3EPA as the linker for the continued study.

Direct use of EtCz3EPA to replace PTAA initially resulted in inferior device performance, mainly because of lower conductivity and hole-extraction capability of EtCz3EPA. The TR decay of EtCz3EPA based samples showed 1.7-fold longer lifetime than the PTAA based sample, confirming the faster hole extraction of PTAA (**Fig. S13**). Because excess holes play a critical role in the UV-accelerated perovskite degradation, we applied an EtCz3EPA/PTAA:BCP hybrid HTM, in which a layer of BCP doped PTAA is coated on EtCz3EPA. This hybrid HTM enhanced device efficiency and stability. BCP was added into PTAA to improve the structural stability of perovskites at the bottom interface through chelation of BCP with lead ion (*2*). However, BCP itself did not enhance the interaction of perovskite with ITO, as BCP did not interact with ITO. The contact angle measurement results showed that $FAPbI_3$ solution had much better wetting on EtCz3EPA than on PTAA:BCP (**Fig. 3C**). The intermediate contact angle of the hybrid HTM suggested that the PTAA:BCP layer on the top of EtCz3EPA is likely non-continuous, as shown in **Fig. 3D**, and provides enough area for the contact of perovskite and the bottom EtCz3EPA.

We conducted atomic force microscope-infrared spectroscopy (AFM-IR) measurements to understand the distribution of HTMs layer on the ITO substrate. The IR signal was collected from

the peak of 1012 or 1028 cm^{-1}, which corresponds to the C-H bending vibrations in -CH_3 group. As shown in **Fig. 3, E** and **F,** and **Fig. S14**, neither PTAA:BCP nor EtCz3EPA exhibited homogeneous coverage on ITO substrate. EtCz3EPA showed a weaker signal as it formed a much thinner layer. PTAA:BCP coated on EtCz3EPA was much less continuous film and left regions exposing EtCz3EPA, which allowed the direct contact of EtCz3EPA with the perovskite (**Fig. 3G**). The diameter of EtCz3EPA region is small enough so that photogenerated holes can still diffuse to PTAA:BCP for efficient collection.

Perovskite films were then deposited onto different HTM to check the bonding strength of perovskites with the ITO/HTM substrates, which was evaluated by our previously established peeling-off method (*9, 35*). The bottom surfaces of perovskites peeled from hybrid HTMs were rougher than those from PTAA:BCP regardless of annealing process, as shown in the SEM images in **Fig. 3, J** and **M**, suggesting that fracture of perovskites occurred in some regions where perovskites stick strongly to ITO during the peel-off process (**Fig. S15, A and B**). Perovskites prepared on PTAA detached at the perovskite/ITO interface. The perovskite films prepared on EtCz3EPA-only or the hybrid HTMs failed cohesively in the perovskite layer, suggesting stronger adhesion of perovskites with ITO and the EtCz3EPA linker. This finding also implied a stronger interaction of EtCz3EPA with both ITO and perovskites than PTAA:BCP. 2PACz-based sample was in between PTAA and EtCz3EPA based samples, and the exposed bottom surface was smoother than that of the EtCz3EPA-based sample (**Fig. S15C**).

Single-lap shear tests were performed to verify the interface bonding strength of perovskite films and ITO/HTMs substrate according to the ASTM D1002 standard (*36*) with the test setup shown in **Fig. S16A**. The observed fracture modes were the same as the peeling off test, as shown by the photos of the fractured films in **Fig. S16B**. The average critical shear stress (σ_c) of PTAA: BCP, 2PACz, and EtCz3EPA based samples are 1.25 MPa, 2.79 MPa and 4.01 MPa respectively (**Fig. 16C**). This result again showed the adhesion of EtCz3EPA with perovskites was strongest among all the HTMs tested, which explains why the EtCz3EPA-based devices had better light-soaking stability under LEP illumination.

Our prior study showed that voids near the embedded interface could be generated after long-term light soaking or thermal annealing mainly because of the recrystallization of amorphous regions in the absorber layer (*9*). Here, we annealed the samples in the dark at 85 °C, which drove the evaporation of residual dimethyl sulfoxide (DMSO) and the recrystallization. For devices with EtCz3EPA-only or hybrid HTMs, the peeled-off perovskite films did not show voids in both pristine samples and after ~1000 hr thermal annealing at 85ºC (**Fig. 3I**, **3J**, **3L**, **3M)**. In contrast, the perovskite film grown on PTAA:BCP showed many voids with size of 30-100 nm formed around the grain boundaries after the annealing process (**Fig. 3K**). Therefore, the perovskites grown on EtCz3EPA are less amorphous, indicating the EtCz3EPA affected the perovskite nucleation and crystallization process. The grazing incident x-ray diffraction patterns in **Fig. S17** showed the enhanced crystallinity of bottom perovskite that was prepared based on ITO/EtCz3EPA substrate.

Improved long-term stability for perovskite solar cells

The J-V curves of the as-prepared and light-soaked devices with different HTMs are shown in **Fig. 4, A** to **C**. After 2-days of testing under LEP light, the PTAA:BCP-based devices showed decreased FF and 9% loss in PCE, whereas the EtCz3EPA based devices showed decreased V_{OC} and only 1% of PCE loss. BCP can only bond to perovskites but has negligible interaction with ITO, leading to a similar variation trend for J-V curves from PTAA:BCP and PTAA based devices. When we did the same measurement to measure the ion migration activation energy with the device structure in **Fig. 2D**, a larger E_a of 546 meV was observed, indicating better crystallinity of perovskite at the bottom interface grown on EtCz3EPA, which is consistent with the GIXRD results (*37, 38*).

After illumination for 50 hr under LEP light, only a slight reduction of E_a (523 meV) was observed, showing stronger bonding reinforced the bottom interface (**Fig. S18**). The PL emission peak mapping of the EtCz3EPA based samples also showed more uniform bandgap distribution than that of PTAA based samples after the LEP light illumination, confirming suppressed cation migration (**Fig. S19**). The PL peak position of fresh samples measured from the top side and bottom side almost overlapped (**Fig. S8E**) and showed a more homogeneous composition along the vertical direction. This result highlighted the importance of the connection between ITO, HTM, and perovskites. Although the trap density of the EtCz3EPA-based device was substantially lower than those of the PTAA:BCP-based devices, trap bands II and III still increased after light soaking (**Fig. 4D-4F**). This result was consistent with the evolution of device efficiency, suggesting that the ITO/perovskite interface has not been effectively stabilized under UV light by BCP addition. The trap density of the EtCz3EPA/PTAA:BCP-based devices did not have a substantially increased after illumination, consistent with J-V results, and could be attributed to the faster hole extraction of the additional PTAA:BCP layer.

The light-soaking stability of these devices with an active area of 8 mm^2 was measured to evaluate the long-term stability. As shown in **Fig. 4G**, the PTAA:BCP based devices showed a T_{90} lifetime of ~3240 hr under LED lamp, which is consistent with our previous result based on lead-chelation capable molecules (*2*). The hybrid HTM based devices had an increased T_{90} lifetime of ~4610 hr. Under LEP light with ~3.5% UV, the PTAA:BCP based devices showed a T_{90} lifetime of ~190 hr, whereas the devices with hybrid HTMs had a T_{90} lifetime of ~1780 hr (**Fig. 4H**).

We also conducted the damp-heat test at 85 ºC and 85% humidity (ISOS-D-3) (*23*) on the PIB encapsulated small devices for 1000 h, which not only examined the encapsulation quality but also the intrinsic heat stability of perovskites (**Fig. 4I**). The devices with all three types of HTMs showed less than 2% efficiency loss after ~1000 hr test. In addition, all of the devices with three types HTMs passed the thermal cycling test with < 2% efficiency loss after 200 thermal cycles between -40º and 85 ºC (**Fig. 4J**).

Outdoor performance testing of perovskite minimodules

We upscaled the HTM coating and fabricated minimodules with an aperture area of 15 to 50 cm^2. As shown in **Fig. 5A**, the minimodule based on hybrid HTM showed an PCE of 22.1% measured near room temperature. This value is comparable to that of the PTAA:BCP based

minimodules (21.6%) after exposed to 1-sun LED lamp for ~100 hr and indicative of good uniformity of the hybrid HTM. The polydimethylsiloxane (PDMS) film was applied as an antireflective layer on the surface of the ITO glass, which increased the photocurrent by ~6% and was removed during the outdoor tests. The minimodules had the same encapsulation as the small-area devices. Although laser scribing area in modules may impose additional degradation pathways. we did not observe reaction of Cu electrode with perovskites after light soaking the minimodules for 4000 hr (**Fig. S20**).

The encapsulated minimodules were then sent to the Perovskite PV Accelerator for Commercializing Technologies (PACT) center for independent outdoor testing (*39*). The minimodule PCEs were measured outdoors in Colorado, USA from May to September of 2023. The minimodules were deployed in the field on a fixed-tilt rack (**Fig. 5B**), and the module surface temperature was monitored daily. Maximum module surface temperature reached 50 ºC during the summer of 2023 (**Fig. S21**). The minimodules were actively loaded at MPP, except at night, when they were kept at short circuit. The irradiance was measured using a broadband thermopile pyranometer and used in efficiency calculations**,** which may yield a different PCE to those measured under solar simulator. There was no temperature, spectrum, angle of incidence, or other corrections applied to field test results to the testing system.

The evolution in device PCE over a single day measured in outdoor conditions. For a daily output evaluation (**Fig. 5C**) showed that the PCE of the champion minimodules stayed at a plateau of > 18% for about 9 hr. As shown in **Fig. 5D** and **Fig. S22**, the operational PCE of the best minimodule remained 17.5% after 10 weeks of outdoor testing in the summer from May 2023, and the average operational efficiency of the minimodules was > 16%. The initial PCE of the minimodule (~15%) at the operational temperature was measured after 7 weeks dark storage between fabrication and field deployment and recovered to ~18% after operation for 6 weeks outdoors. The daily PCE of the minimodules increased for the first several weeks of testing before it began to decline, which is a normal light-soaking effect of this perovskite composition. The daily PCE of the best minimodule installed from September 2023 remained > 16% after 29 weeks of outdoor testing (**Fig. S23**). This is the longest-lasting minimodule tested at the PACT center to date (*40*).

The device's PCE measured in the testing field is different from those measured at room-temperature indoor testing because of the different light intensity, light spectrum, and temperature. The perovskite temperature was higher than module surface temperature because the perovskites were heated by sun light. We used a hot plate to control the module surface temperature to be between 40º and 50 ºC, where the module was covered by a glass container to minimize airflow, and found the perovskite temperature was measured to 8º to 10 ºC higher using a solar simulator and a perovskite minimodule with the same size and encapsulation (**Fig. S24**). The temperature difference of perovskites and module surface may be slightly different in field.

We tested how sensitive these modules are to light intensity and temperature using minimodules fabricated by the same process. As shown in **Fig. S25** and **S26**, the PCE of minimodules was almost constant with light intensity from 20 to 100 mW cm^{-2}. However, but they

showed a temperature coefficient of -0.32% $^{o}C^{-1}$, which is still better than that of silicon solar cells but larger than has been reported for $MAPbI_3$-based minimodules (*41*).

Discussion

We identified the UV-induced perovskite degradation mechanism and showed that introduction of a stronger interconnection layer to the devices improved the outdoor stability of the perovskite minimodules. UV light directly damaged the interface of perovskite and the substrate, which resulted in inefficient hole extraction and accelerated the A-site cation migration. The introduction of stronger bonding molecules at the buried interface reduced the amorphous phase around perovskite/HTM/ITO region and suppressed cation migration under UV light. With the hybrid HTM, EtCz3EPA/PTAA:BCP, in the small-area perovskite solar cells, the T_{90} lifetimes measured under LED and LEP lamp were increased to ~4610 and ~1780 hr, respectively. The champion minimodule with the hybrid HTM retained operational efficiency of > 16% after 29 weeks of outdoor testing independently measured by PACT center.

Acknowledgments:

Funding: This material is based upon work supported by the U.S. Department of Energy's Office of Energy Efficiency and Renewable Energy (EERE) under the Solar Energy Technologies Office Award Number DE-EE0009520. PACT testing is supported by the U.S. Department of Energy's Office of Energy Efficiency and Renewable Energy (EERE) under the Solar Energy Technologies Office Award Number 38050. The outdoor stability testing was authored by the National Renewable Energy Laboratory, operated by Alliance for Sustainable Energy, LLC, for the U.S. Department of Energy (DOE) under Contract No. DE-AC36-08GO28308. Portion of the optical characterizations and DFT calculation was supported by the Center for Hybrid Organic Inorganic Semiconductors for Energy (CHOISE), an Energy Frontier Research Center funded by the Office of Basic Energy Sciences, Office of Science within the US Department of Energy. The nanoprobe X-ray fluorescence measurements were supported in part by the U.S. Department of Energy's Office of Energy Efficiency and Renewable Energy (EERE) under the Solar Energy Technologies Office Award Number DE-EE0009527 and in part by the National Science Foundation under award DMR-1848371. The views expressed herein do not necessarily represent the views of the U.S. Department of Energy or the United States Government.

Author contributions: C.F. and J.H. conceived the idea. C.F. fabricated and characterized perovskite films and devices. A.K. and A.S. designed, synthesized, and characterized the HTM molecule EtCz3EPA. C.F. and J.H. also participated in the design of EtCz3EPA. X.S. fabricated some of the minimodules for outdoor stability evaluation. M.W. performed the GIXRD measurements and acquired the SEM images. Z.S. carried out the PL mapping of the samples. H.J. carried out the AFM-IR measurement and analysis. T.J.S., M.O-B. and L.T. S. carried out the outdoor test. Y.D., R.S., M.C.B. measured the TR spectrums and did the analysis. H.G. did the UV-vis absorption measurement. G.Y. carried out the tDOS analysis.

N.L. established the light cycling stability test system. Y.X., X.W. and Y.Y. did the DFT calculations. C.J.D., Z.J.D., D.N.C and D.P.F. carried out the XRF measurement and analysis. C.F. and J.H. wrote the manuscript, and all authors commented on the manuscript.

Competing interests: C.F., A.K., A.S. and J.H. are authors of a provisional patent based on this manuscript. Tandem PV is an entity to which the following technologies used or evaluated in this paper have been licensed: an ink formulation for fast coating of perovskites and BHC for reducing iodine. J.H. is an inventor of technologies and has received royalties. These relationships have been disclosed to and are under management by UNC-Chapel Hill.

Data and materials availability: All data are available in the main text or the supplementary materials.

Supplementary Materials

Materials and Methods

Figs. S1 to S26

Tables S1 to S4

References and Notes

1. J. Park *et al.*, Controlled growth of perovskite layers with volatile alkylammonium chlorides. *Nature* **616**, 724-730 (2023).
2. C. Fei *et al.*, Lead-chelating hole-transport layers for efficient and stable perovskite minimodules. *Science* **380**, 823-829 (2023).
3. Y. Zhao *et al.*, Inactive $(PbI_2)_2RbCl$ stabilizes perovskite films for efficient solar cells. *Science* **377**, 531-534 (2022).
4. G. Grancini *et al.*, One-Year stable perovskite solar cells by 2D/3D interface engineering. *Nat. Commun.* **8**, 15684 (2017).
5. C. Li *et al.*, Rational design of Lewis base molecules for stable and efficient inverted perovskite solar cells. *Science* **379**, 690-694 (2023).
6. X. Zhao *et al.*, Accelerated aging of all-inorganic, interface-stabilized perovskite solar cells. *Science* **377**, 307-310 (2022).
7. M. Wang *et al.*, Ammonium cations with high pKa in perovskite solar cells for improved high-temperature photostability. *Nat. Energy* **8**, 1229-1239 (2023).
8. N. Li *et al.*, Liquid medium annealing for fabricating durable perovskite solar cells with improved reproducibility. *Science* **373**, 561-567 (2021).
9. M. Wang, C. Fei, M. A. Uddin, J. Huang, Influence of voids on the thermal and light stability of perovskite solar cells. *Sci. Adv.* **8**, eabo5977 (2022).
10. X. Zheng *et al.*, Co-deposition of hole-selective contact and absorber for improving the processability of perovskite solar cells. *Nat. Energy* **8**, 462-472 (2023).
11. J. Yin, X. Shi, L. Wang, H. Yan, S. Chen, High-Performance Inverted Perovskite Solar Devices Enabled by a Polyfullerene Electron Transporting Material. *Angew. Chem. Int. Ed.* **61**, e202210610 (2022).
12. N. U. Rahman *et al.*, A promising europium-based down conversion material: organic–inorganic perovskite solar cells with high photovoltaic performance and UV-light stability. *J. Mater. Chem. A* **7**, 6467-6474 (2019).

13. L. Shi *et al.*, Gas chromatography-mass spectrometry analyses of encapsulated stable perovskite solar cells. *Science* **368**, eaba2412 (2020).
14. T. Wang *et al.*, Room temperature nondestructive encapsulation via self-crosslinked fluorosilicone polymer enables damp heat-stable sustainable perovskite solar cells. *Nat. Commun.* **14**, 1342 (2023).
15. X. Xiao *et al.*, Lead-adsorbing ionogel-based encapsulation for impact-resistant, stable, and lead-safe perovskite modules. *Sci. Adv.* **7**, eabi8249 (2021).
16. H. Hussain *et al.*, Structure of a model TiO_2 photocatalytic interface. *Nat. Mater.* **16**, 461-466 (2017).
17. R. Liu, L. Wang, Y. Fan, Z. Li, S. Pang, UV degradation of the interface between perovskites and the electron transport layer. *RSC Adv.* **10**, 11551-11556 (2020).
18. W. Li, J. Li, G. Niu, L. Wang, Effect of cesium chloride modification on the film morphology and UV-induced stability of planar perovskite solar cells. *J. Mater. Chem. A* **4**, 11688-11695 (2016).
19. J. Ji *et al.*, Two-Stage Ultraviolet Degradation of Perovskite Solar Cells Induced by the Oxygen Vacancy-Ti^{4+} States. *iScience* **23**, 101013 (2020).
20. M. Petrović *et al.*, Limitations of a polymer-based hole transporting layer for application in planar inverted perovskite solar cells. *Nanoscale Adv.* **1**, 3107-3118 (2019).
21. J. H. Park, O. J. Kwon, T.-H. Kim, J. Mun, Y. D. Park, Ultraviolet irradiation creates morphological order via conformational changes in polythiophene films. *Org. Electron.* **62**, 394-399 (2018).
22. Y. Deng *et al.*, Defect compensation in formamidinium-caesium perovskites for highly efficient solar mini-modules with improved photostability. *Nat. Energy* **6**, 633-641 (2021).
23. M. V. Khenkin *et al.*, Consensus statement for stability assessment and reporting for perovskite photovoltaics based on ISOS procedures. *Nat. Energy* **5**, 35-49 (2020).
24. R. A. Kerner, B. P. Rand, Electrochemical and Thermal Etching of Indium Tin Oxide by Solid-State Hybrid Organic-Inorganic Perovskites. *ACS Appl. Energy Mater.* **2**, 6097-6101 (2019).
25. Q. Jiang *et al.*, Towards linking lab and field lifetimes of perovskite solar cells. *Nature* **623**, 313-318 (2023).
26. Z. Liang *et al.*, Homogenizing out-of-plane cation composition in perovskite solar cells. *Nature* **624**, 557-563 (2023).
27. Z. Ni *et al.*, Resolving spatial and energetic distributions of trap states in metal halide perovskite solar cells. *Science* **367**, 1352-1358 (2020).
28. Z. Ni *et al.*, Evolution of defects during the degradation of metal halide perovskite solar cells under reverse bias and illumination. *Nat. Energy* **7**, 65-73 (2022).
29. J. Ye *et al.*, Defect Passivation in Lead-Halide Perovskite Nanocrystals and Thin Films: Toward Efficient LEDs and Solar Cells. *Angew. Chem. Int. Ed.* **60**, 21636-21660 (2021).
30. Y. Lin *et al.*, Excess charge-carrier induced instability of hybrid perovskites. *Nat. Commun.* **9**, 4981 (2018).
31. Y. Lin *et al.*, Self-Assembled Monolayer Enables Hole Transport Layer-Free Organic Solar Cells with 18% Efficiency and Improved Operational Stability. *ACS Energy Lett.* **5**, 2935-2944 (2020).
32. A. Al-Ashouri *et al.*, Conformal monolayer contacts with lossless interfaces for perovskite single junction and monolithic tandem solar cells. *Energy Environ. Sci.* **12**, 3356-3369 (2019).

33. B. Abdollahi Nejand *et al.*, Scalable two-terminal all-perovskite tandem solar modules with a 19.1% efficiency. *Nat. Energy* **7**, 620-630 (2022).
34. R. Lin *et al.*, All-perovskite tandem solar cells with 3D/3D bilayer perovskite heterojunction. *Nature* **620**, 994-1000 (2023).
35. S. Chen *et al.*, Stabilizing perovskite-substrate interfaces for high-performance perovskite modules. *Science* **373**, 902-907 (2021).
36. T. R. Guess, R. E. Allred, F. P. Gerstle, Jr., Comparison of Lap Shear Test Specimens. *J. Test. Eval.* **5**, 84-93 (1977).
37. Y. Yuan, J. Huang, Ion Migration in Organometal Trihalide Perovskite and Its Impact on Photovoltaic Efficiency and Stability. *Acc. Chem. Res.* **49**, 286-293 (2016).
38. J. Huang, Y. Yuan, Y. Shao, Y. Yan, Understanding the physical properties of hybrid perovskites for photovoltaic applications. *Nat. Rev. Mater.* **2**, 17042 (2017).
39. PACT, PACT Perovskite PV Module Outdoor Test Protocol. 2024 https://pvpact.sandia.gov/download/1305/.
40. PACT, PACT field performance plot. 2024 https://pvpact.sandia.gov/results-and-data/.
41. Y. Deng *et al.*, Tailoring solvent coordination for high-speed, room-temperature blading of perovskite photovoltaic films. *Sci. Adv.* **5**, eaax7537 (2019).

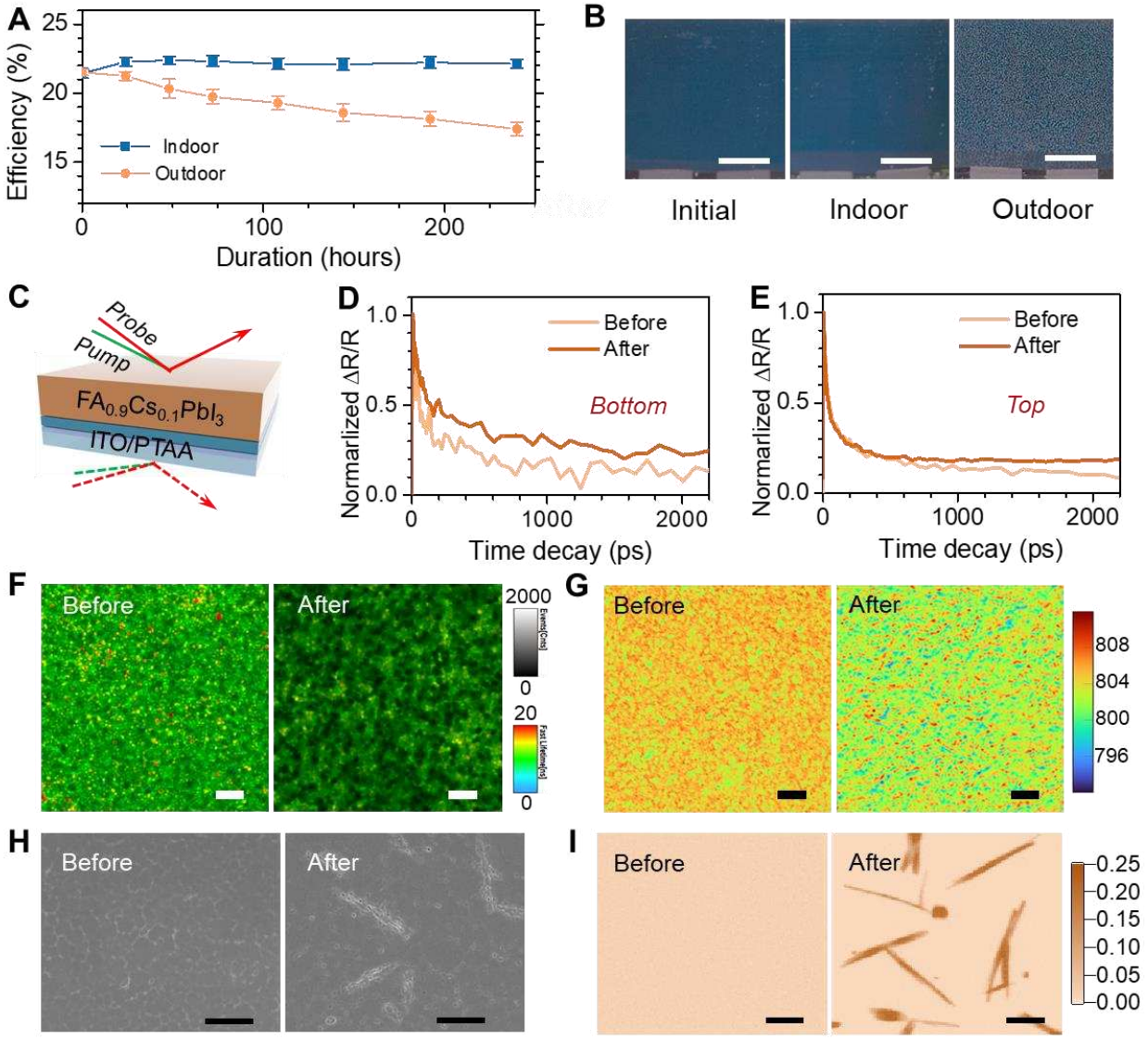

Fig. 1. Perovskite degradation in indoor and outdoor conditions. (A) Indoor and outdoor light soaking stability of perovskite solar cells. The devices tested indoors were under LED lamp (100 mW cm^{-2}, with <0.1% UV inside, 60±5 ºC, OC conditions) and those tested outdoors were under sunlight and ~20 ºC average daytime temperature (North Carolina, US). (B) Photographs of the perovskite solar cells (ITO/HTM side) before and after indoor and outdoor tests. The scale bars are 2 mm. (C) Illustration for the transient reflection spectroscopy (TR) test of the perovskite films; The TR decay of the LEP lamp illuminated perovskite films (100 mW cm^{-2}, with ~3.5% UV inside, 60±5 ºC, OC conditions) tested from the (D) bottom and (E) top side. (F) Photoluminescence (PL) intensity-lifetime mapping and (G) the corresponding PL emission peak wavelength mapping of the PTAA based perovskite films before and after LEP lamp illumination for ~100 hr. The images were collected from the bottom side and the scale bars are 10 μm. (H) Scanning electron microscopy (SEM) images of the bottom perovskite layer before and after LEP light illumination for ~200 hr. The scale bars are 5 μm. (I) X-ray fluorescence (XRF) mapping of the Cs/I ratio of the bottom perovskite layer before and after light illumination. The scale bars are 5 μm.

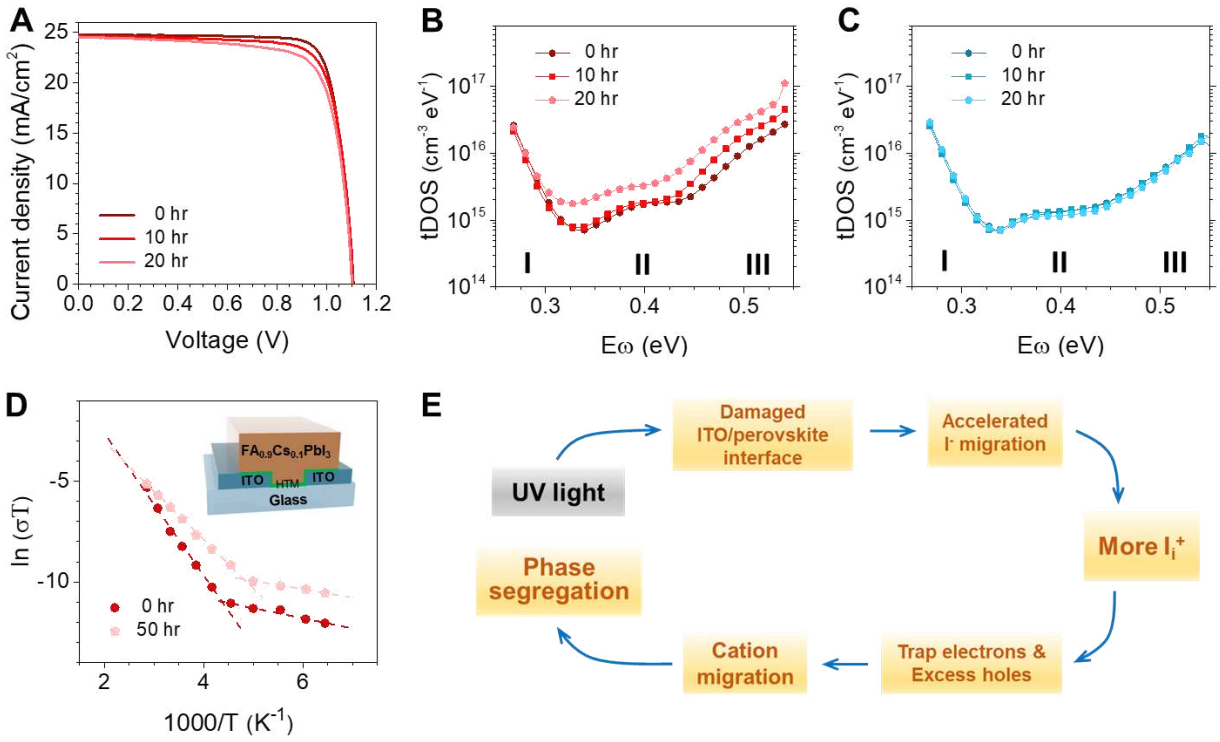

Fig. 2. Mechanism of UV induced perovskite degradation. (A) J-V curves of PTAA based small devices illuminated under LEP light (100 mW cm^{-2}, with ~3.5% UV inside, ~60 ºC, OC conditions) at the initial stage; Trap density of PTAA based perovskite solar cells illuminated by (B) LEP lamp and (C) LED lamp for different time; (D) Temperature-dependent dark conductivity of the lateral structure devices before and after 50 hr illumination under the LEP lamp. The inset is the sample configuration. (E) Schematic degradation process of perovskite under light illumination with strong UV light.

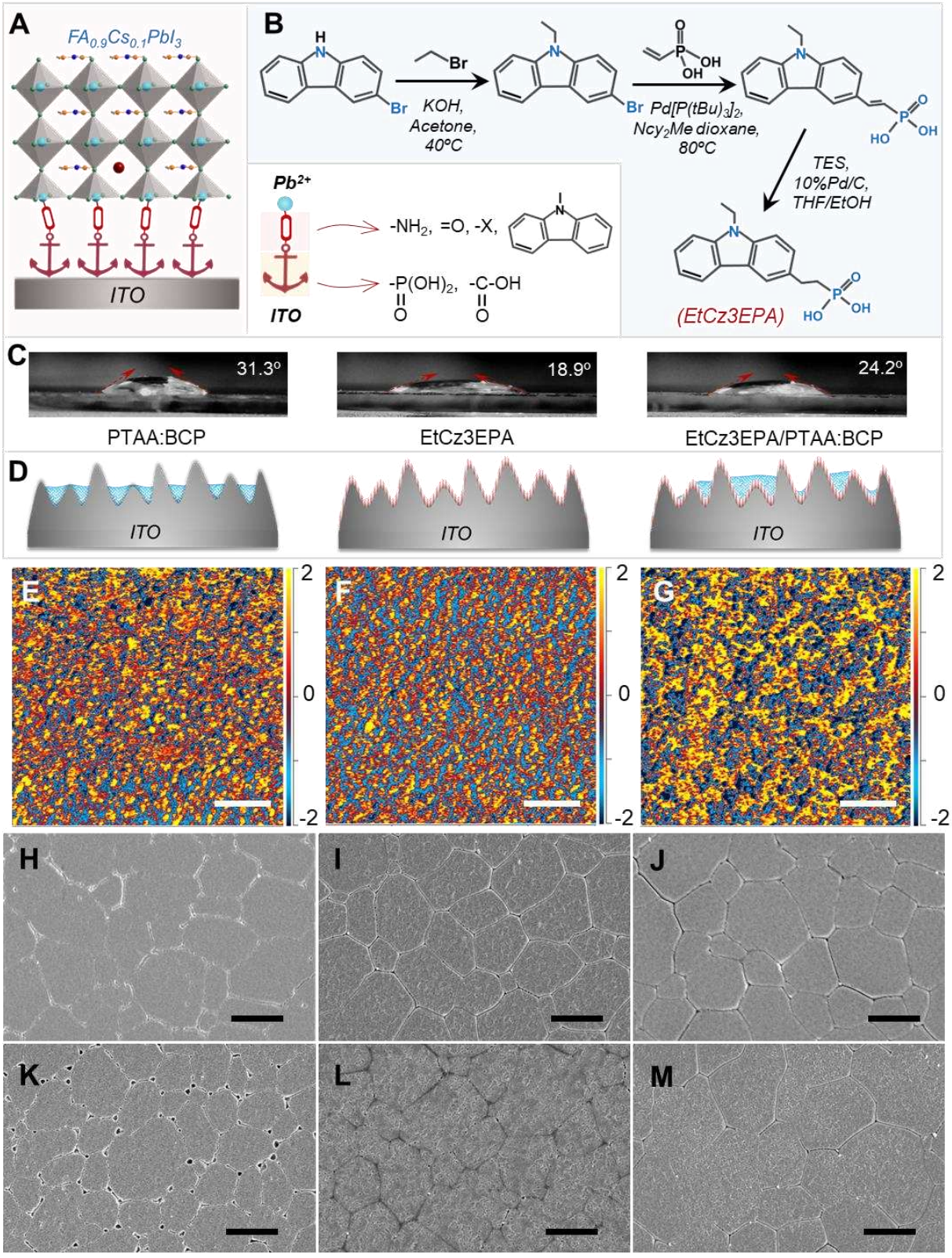

Fig. 3. Molecular design for stronger bonding HTM. (A) Schematic interfacial contact of perovskite, bifunctional molecular and ITO substrate. (B) Synthesis route of EtCz3EPA. (C) Contact angle of $FAPbI_3$ solution (1M, dissolved in 2-ME) on different HTM substrates. (D)

Illustration for the different HTMs on the ITO substrate. Atomic force microscope-infrared spectroscopy (AFM-IR) of different HTMs on ITO substrates: (E) PTAA:BCP, (F) EtCz3EPA and (G) the hybrid HTM. The images were collected at the wavenumbers of 1028, 1012 and 1028 cm^{-1}, respectively, corresponding to C-H bending in the $-CH_3$ groups. The scale bars in the images are 1 μm. SEM images of the bottom morphology of perovskite layer peeled from different ITO/HTM substrate (H-J) before and (K-M) after ~1000 hr annealing process under 85ºC in dark. (H) and (K) are PTAA:BCP based samples, (I) and (L) are EtCz3EPA based samples, (J) and (M) are the hybrid HTM based samples. The scale bars in the images are 2 μm.

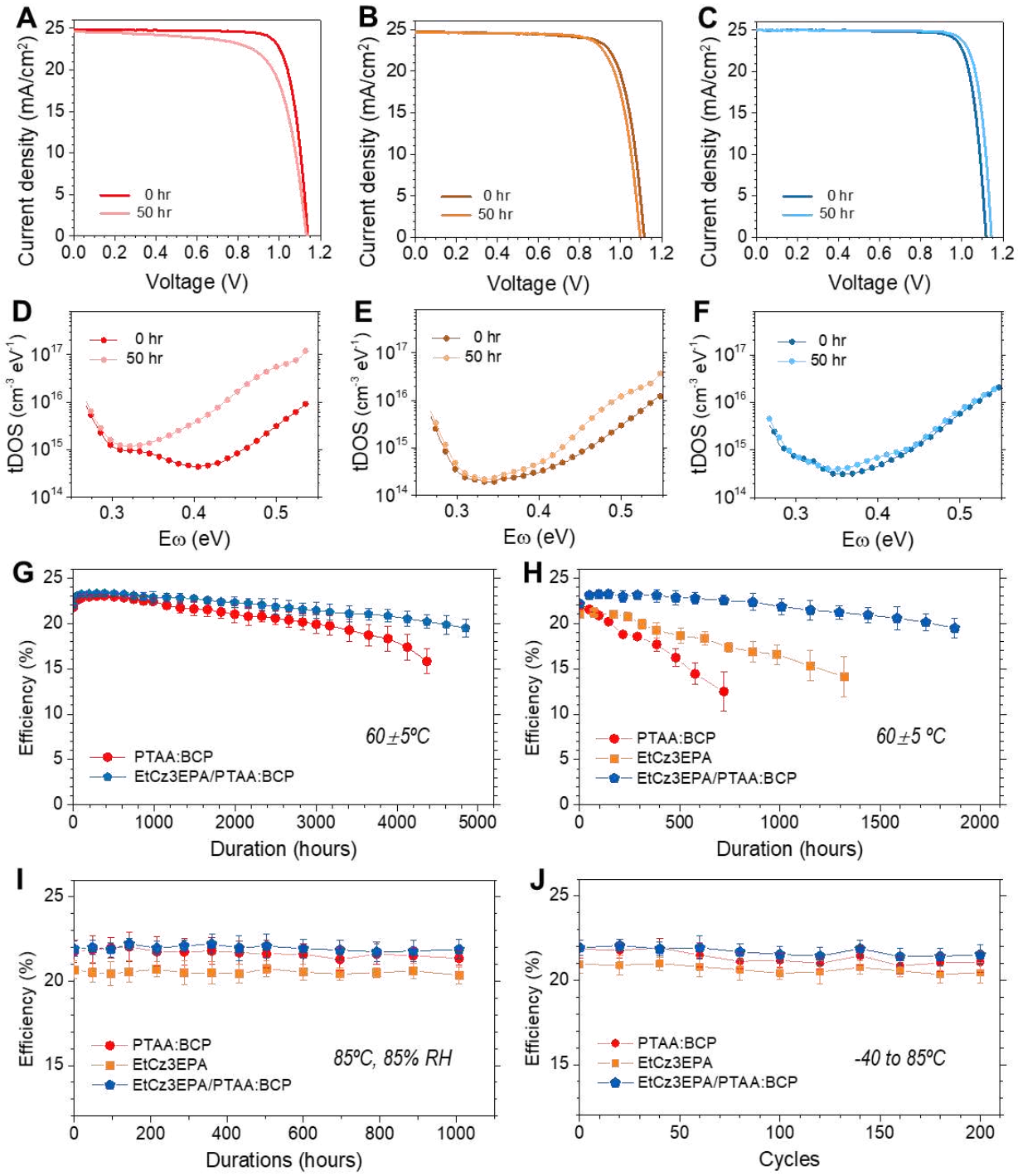

Fig. 4. Long-term stability of perovskite solar cells. J-V curves of small devices (0.08 cm^2) with different HTMs and 50 hr LEP light soaking: (A) PTAA:BCP, (B) EtCz3EPA and (C) the hybrid HTM. The corresponding trap density of perovskite solar cells based on (D) PTAA:BCP, (E) EtCz3EPA and (F) the hybrid HTM and illuminated by LEP lamp for 50 hr. Light soaking stability of small area devices (OC conditions, 60±5 ºC) based on different HTM layers under the illumination of (G) LED lamp and (H) LEP lamp. The light intensities of the lamps were calibrated to 100 mW cm^{-2}. (I) Damp heat test under 85 ºC and 85% humidity (ISOS-D-3) of the small devices

for ~1000 hr; (J) Thermal cycling test between -40 to 85ºC of the small devices for 200 cycles; All the data for the small devices in the long-term stability test were collected from 20 to 30 devices for each group.

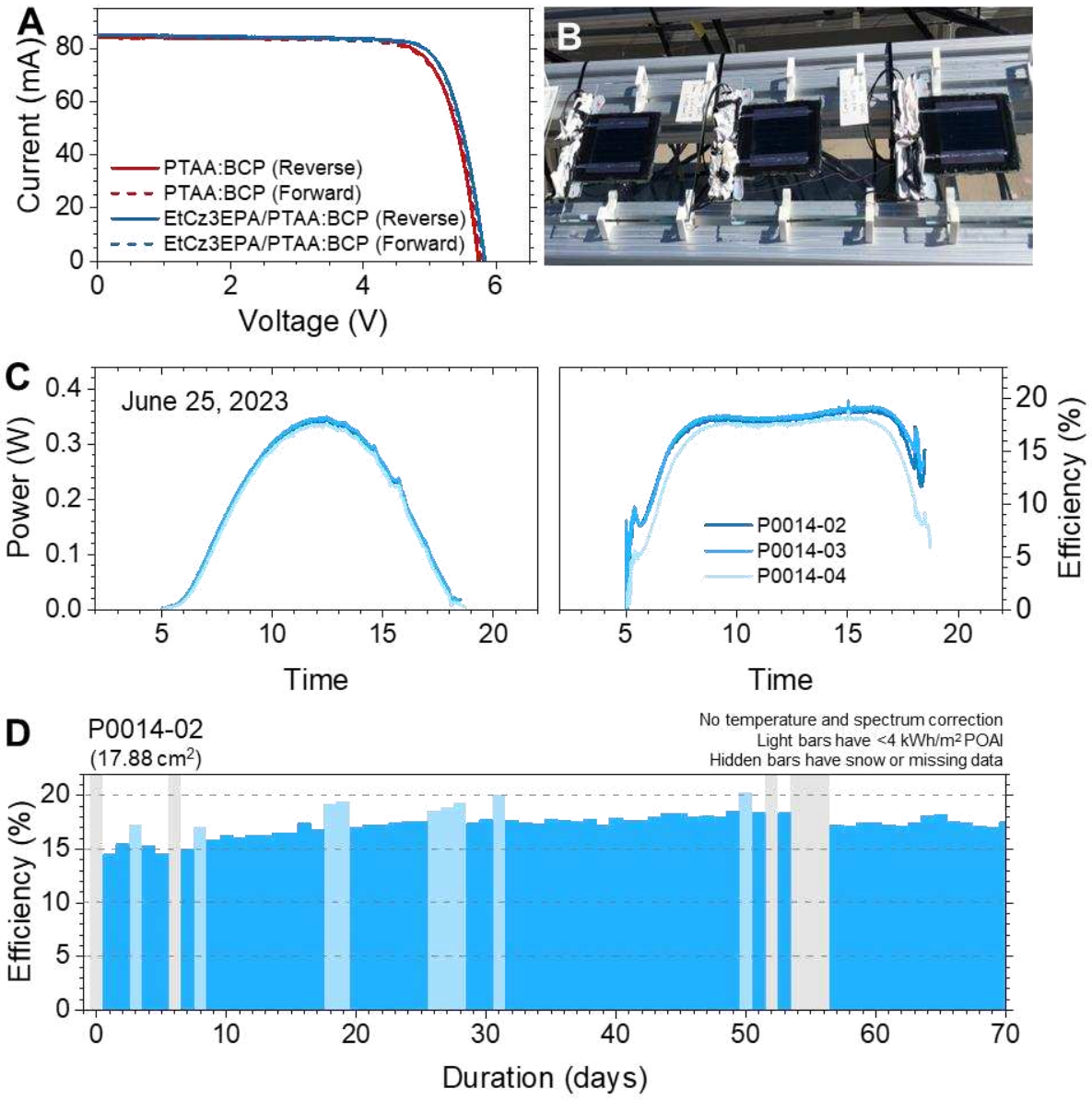

Fig. 5. Outdoor test of perovskite minimodules (A) J-V curves of the minimodules based on PTAA:BCP and the hybrid HTMs. The minimodules with an aperture area of 17.88 cm^2 and PDMS antireflection layers have been pre-soaked under LED lamp for ~100 hr to achieve highest efficiency. (B) A typical photograph of the outdoor stability testing system for perovskite modules; (C) The daily output power and efficiency of the minimodules on June 25, 2023. (D) Outdoor test of hybrid HTM based perovskite minimodule measured by PACT center. The minimodule was measured without PDMS antireflection layer and stored in dark for ~7 weeks before testing outdoor. The daily efficiency is calculated by the daily energy delivered by the photovoltaic device divided by the daily energy incident on the device. The incident power is the irradiance measured by a broadband pyranometer multiplied by the device aperture area.